A search for $\nu_\mu \to \nu_\tau$ oscillations using the NOMAD detector

NOMAD Collaboration

J. Altegoer [f], C. Angelini [q], P. Astier [o], D. Autiero [i], A. Baldisseri [s],
M. Baldo-Ceolin [n], G. Ballocchi [i], M. Banner [o], S. Basa [j], G. Bassompierre [b],
K. Benslama [j], N. Besson [s], I. Bird [i,j], B. Blumenfeld [c], F. Bobisut [n], J. Bouchez [s],
S. Boyd [u], A. Bueno [d,x], S. Bunyatov [g], L. Camilleri [i], A. Cardini [k], A. Castera [o],
P.W. Cattaneo [p], V. Cavasinni [q], A. Cervera-Villanueva [i], G. Collazuol [n],
G. Conforto [v], C. Conta [p], M. Contalbrigo [n], R. Cousins [k], D. Daniels [d],
H. Degaudenzi [j], T. Del Prete [q], A. De Santo [q], T. Dignan [d], L. Di Lella [i],
E. do Couto e Silva [i], I.J. Donnelly [t,u], J. Dumarchez [o], T. Fazio [b], G.J. Feldman [d],
R. Ferrari [p], D. Ferrère [i], V. Flaminio [q], M. Fraternali [p], G. Fumagalli [p,1],
J.-M. Gaillard [b], P. Galumian [j], E. Gangler [i,o], A. Geiser [i], D. Geppert [f], D. Gibin [n],
S. Gninenko [m], J.-J. Gomez-Cadenas [a,i], J. Gosset [s], C. Gößling [f], M. Gouanère [b],
A. Grant [i], G. Graziani [h], A. Guglielmi [n], C. Hagner [s], J. Hernando [a,2],
D. Hubbard [d], P. Hurst [d], N. Hyett [l], E. Iacopini [h], C. Joseph [j], F. Juget [j],
D. Kekez [w], B. Khomenko [i], M. Kirsanov [m], O. Klimov [g], J. Kokkonen [i],
A. Kovzelev [m], V.E. Kuznetsov [g], S. Lacaprara [n], A. Lanza [p], L. La Rotonda [e],
M. Laveder [n], C. Lazzeroni [q], A. Letessier-Selvon [o], J.-M. Levy [o], L. Linssen [i],
A. Ljubičić [w], J. Long [c,3], A. Lupi [h], E. Manola-Poggioli [b,i], A. Marchionni [h],
F. Martelli [v], X. Méchain [s], J.-P. Mendiburu [b], J.-P. Meyer [s], M. Mezzetto [n],
S.R. Mishra [d], G.F. Moorhead [l], L. Mossuz [b], P. Nédélec [b,i], Yu. Nefedov [g],
C. Nguyen-Mau [j], D. Orestano [r], F. Pastore [r], L.S. Peak [u], E. Pennacchio [v],
J-P. Perroud [j], H. Pessard [b], R. Petti [p], A. Placci [i], H. Plothow-Besch [i], A. Pluquet [s],
G. Polesello [p], D. Pollmann [f], B.G. Pope [i], B. Popov [g], C. Poulsen [l], P. Rathouit [s],
G. Renzoni [q], C. Roda [i,q], A. Rubbia [i,x], F. Salvatore [p], D. Scannicchio [p],
K. Schahmaneche [o], B. Schmidt [f], A. Sconza [n], M. Serrano [o], M. Sevior [l],
D. Sillou [b], F.J.P. Soler [u], G. Sozzi [j], D. Steele [c,j], P. Steffen [i], M. Steininger [j],
U. Stiegler [i], M. Stipčević [w], Th. Stolarczyk [s], M. Tareb-Reyes [j], G.N. Taylor [l],
V. Tereshchenko [g], A. Toropin [m], A.-M. Touchard [o], S.N. Tovey [i,l], M.-T. Tran [j],
E. Tsesmelis [i], J. Ulrichs [u], V. Uros [o], L. Vacavant [j], M. Valdata-Nappi [e,4],

V. Valuev [g], F. Vannucci [o], K.E. Varvell [t,u], M. Veltri [v], V. Vercesi [p],
D. Verkindt [b], J.-M. Vieira [j], T. Vinogradova [k], M.-K. Vo [s], S. Volkov [m],
F.V. Weber [d,i], T. Weisse [f], M. Werlen [j], F.F. Wilson [i], L.J. Winton [l],
B.D. Yabsley [u], H. Zaccone [s], K. Zuber [f]

[a] *University of Massachusetts, Amherst, MA, USA*
[b] *LAPP, Annecy, France*
[c] *Johns Hopkins University, Baltimore, MD, USA*
[d] *Harvard University, Cambridge, MA, USA*
[e] *University of Calabria and INFN, Cosenza, Italy*
[f] *Dortmund University, Dortmund, Germany*
[g] *JINR, Dubna, Russia*
[h] *University of Florence and INFN, Florence, Italy*
[i] *CERN, Geneva, Switzerland*
[j] *University of Lausanne, Lausanne, Switzerland*
[k] *UCLA, Los Angeles, CA, USA*
[l] *University of Melbourne, Melbourne, Australia*
[m] *Institute for Nuclear Research (INR), Moscow, Russia*
[n] *University of Padova and INFN, Padova, Italy*
[o] *LPNHE, University of Paris, Paris VI and VII, France*
[p] *University of Pavia and INFN, Pavia, Italy*
[q] *University of Pisa and INFN, Pisa, Italy*
[r] *Roma Tre University / INFN, Rome, Italy*
[s] *DAPNIA, CEA Saclay, France*
[t] *ANSTO Sydney, Menai, Australia*
[u] *University of Sydney, Sydney, Australia*
[v] *University of Urbino, Urbino, and INFN Florence, Italy*
[w] *Rudjer Bošković Institute, Zagreb, Croatia*
[x] *ETH Zürich, Zürich, Switzerland*

Abstract

NOMAD is a neutrino oscillation experiment designed to search for ν_τ appearance in the CERN-SPS wide band ν_μ beam. Signal detection relies on the identification of ν_τ charged current interactions using kinematic criteria. The analysis of the 1995 data sample yields no oscillation signal. Combining all studied τ decay modes, a limit of $\sin^2 2\theta_{\mu\tau} < 4.2 \times 10^{-3}$ is obtained for large Δm^2 at the 90% confidence level. © 1998 Elsevier Science B.V. All rights reserved.

1. Introduction

The field of neutrino physics is rich in unsolved anomalies which could be explained by massive neutrinos and neutrino oscillations [1]. All experiments measuring the flux of solar neutrinos observe a deficit compared to the prediction of solar models. The ratio of muon to electron events observed in atmospheric neutrino interactions is measured by most experiments to be less than expected from models of cosmic ray interactions in the atmosphere. The LSND experiment has observed possible oscillation signals in the $\bar{\nu}_\mu - \bar{\nu}_e$ and $\nu_\mu - \nu_e$ channels [2].

---

[1] Deceased.
[2] Now at UCSC, Santa Cruz, CA, USA.
[3] Now at University of Colorado, Boulder, CO, USA.
[4] Now at University of Perugia, Perugia, Italy.

Finally various astrophysical observations indicate the existence of non-luminous matter in the universe, a prime candidate for which is the relic neutrinos from the big bang provided their mass is a few eV/c^2. These observations make the search for neutrino oscillations a very worthwhile endeavour.

This letter describes a search for $\nu_\mu - \nu_\tau$ oscillations in the predominantly ν_μ CERN-SPS wide band beam using the appearance method. The experiment is sensitive to the cosmologically relevant mass range [3] ($\delta m^2 > 1$ eV^2/c^4) and to mixing angles about an order of magnitude smaller than the best limit available at the time of the NOMAD proposal [4] ($\sin^2 2\theta < 5 \times 10^{-3}$ at high δm^2), set by the E531 experiment [5].

Potential ν_τ candidates are identified through their charged current (CC) interaction. NOMAD is designed to detect both the leptonic ($e^- \bar{\nu}_e \nu_\tau$ or $\mu^- \bar{\nu}_\mu \nu_\tau$) and hadronic (1-prong or 3-prong) decay modes of the produced τ^-. The ν_τ interactions are recognized through kinematic criteria based on the isolation of the τ decay products from the remainder of the event and on the momentum imbalance in the transverse plane (missing p_T) induced by the momentum carried away by the final state neutrino(s) from τ decay.

This method imposes stringent requirements on the design of the detector. Electrons and muons need to be well identified to search for τ's in the leptonic

modes as well as for rejecting CC background as efficiently as possible in the $\tau \rightarrow$ hadrons search. The energy of neutral particles and the momentum of charged particles needs to be measured as precisely as possible in order to have good missing p_T resolution.

2. The detector

A side view of the NOMAD setup is shown in Fig. 1 and a detailed description of the detector can be found elsewhere [6]. We describe briefly its main components. The NOMAD detector consists of a number of subdetectors most of which are located in a dipole magnet with a field volume of $7.5 \times 3.5 \times 3.5$ m^3. The target part of the detector was designed to accommodate two conflicting requirements: to be as light as possible (low density and low atomic number materials) in order to allow the precise measurement of charged particle momenta and to minimize electromagnetic showers and hadronic interactions, and to be as heavy as possible in order to produce a significant number of neutrino interactions.

This conflict was resolved using an active target (2.7 tons) of 44 3×3 m^2 drift chambers (DC) perpendicular to the beam axis, with the target mass
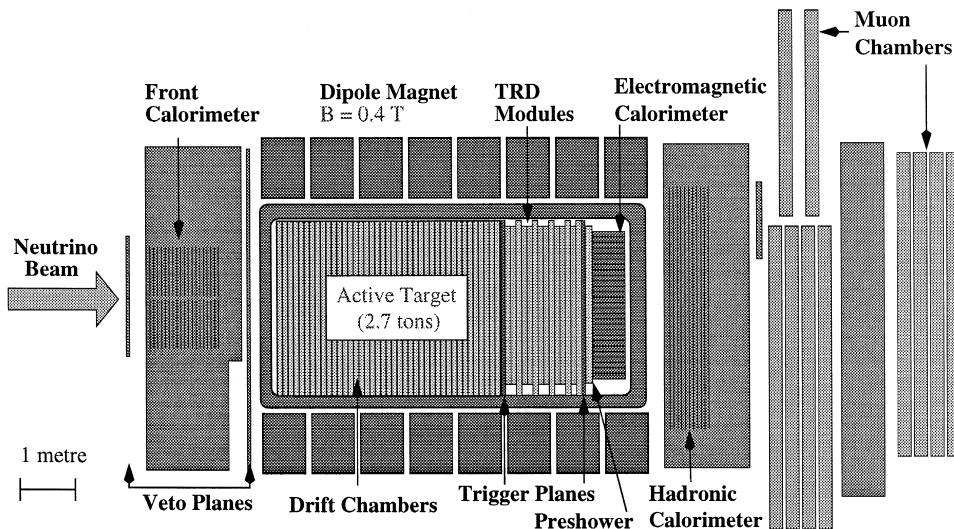

Fig. 1. Side view of the NOMAD detector.

(mainly carbon) given by the chamber structure with an average density of 0.1 g/cm^3. Placed inside the magnetic field of 0.4 T, these chambers provide a momentum resolution of

$$\frac{\sigma_p}{p} \approx \frac{0.05}{\sqrt{L}} \oplus \frac{0.008 \times p}{\sqrt{L^5}},$$

where L is the track length in meters, and p is the momentum in GeV/c. This corresponds to a resolution of 3.5% for average length tracks with momenta up to 20 GeV/c. The drift chambers are followed by 9 transition radiation modules (TRD) [7]. Each module consists of a polypropylene radiator followed by a plane of straw tubes. Five additional drift chambers are interleaved with the TRD modules. Two scintillator trigger planes, T1 and T2, are placed before and after the TRD. Together with a veto scintillation plane V, placed in front of the magnet, they provide the trigger $\overline{V}$T1T2. A preshower (PS), consisting of a 1.6 radiation length (X_0) lead converter and a horizontal and a vertical plane of proportional tubes, follows the TRD and precedes an electromagnetic calorimeter (ECAL) [8] consisting of an array (19 X_0) of lead glass Čerenkov counters. The energy resolution of the PS/ECAL system is $\sigma(E)/E = 3.2\%/\sqrt{E(\text{GeV})} \oplus 1\%$. The combination of the TRD information with tracking and calorimetry yields excellent electron identification as described below.

An iron-scintillator hadronic calorimeter (HCAL) with an energy resolution of $100\%/\sqrt{E(\text{GeV})}$ is located just outside the magnet coil and is followed by two muon detection stations consisting of large area drift chambers, the first after 8 and the second after 13 interaction lengths (λ_0). They provide segments and hits which can be associated to extrapolated DC tracks.

3. The neutrino beam

The CERN-SPS wide band beam is produced by 450 GeV/c protons impinging on a beryllium target. The resulting positive particles are focused into a quasi parallel beam by a system of magnetic horns and allowed to decay in a 290 m long evacuated tunnel followed by an earth and iron shield. The neutrinos are produced at an average distance of 625 m from the detector. In the absence of oscillations the relative beam composition in $\nu_\mu{:}\bar{\nu}_\mu{:}\nu_e{:}\bar{\nu}_e$ is 1:0.07:0.01:0.003 with corresponding average energies of 23.6, 22.7, 37.0 and 33.2 GeV [6]. Note that the smallness of the ν_e component makes the search for $\tau^- \to e^- \bar{\nu}_e \nu_\tau$ particularly sensitive as few ν_e CC background events will be produced. Direct contamination by ν_τ's from the decay of D_s mesons produced at the beryllium target is estimated to be in the 5×10^{-6} range [9], and therefore negligible compared to the sensitivity of the experiment.

4. The data sample

This analysis is based on data collected during the first NOMAD run in 1995, for a total exposure of 0.86×10^{19} protons on target (p.o.t.). During that year the drift chambers were installed in 3 stages, so that the running time was divided into 3 nearly equal periods in which 16, then 32, then the full 44 target chambers were in place. During the analysis, events from the target were selected by requiring a vertex consisting of at least 2 tracks inside the fiducial area $|x| < 130$ cm and $-125 < y < 135$ cm, where x and y are the horizontal and vertical detector axes perpendicular to the beam. In the direction along the longitudinal detector axis, z, which coincides with the beam direction up to a rotation of 42 mrad in the $y - z$ plane, the vertex was required to be at least 5 cm into the target. This yields 130 000 events with an identified muon which, given the muon detection efficiency of 80%, corresponds to 162 000 ν_μ CC events. The overall data sample therefore includes these events and correspondingly smaller numbers of neutral current (NC) events and of events produced by other neutrino flavours.

For studies of low multiplicity events including quasielastic neutrino interactions, a special event selection was made also allowing a single visible track in a slightly reduced fiducial volume.

Monte Carlo (MC) events are generated according to the expected neutrino flux using a deeply inelastic (DIS) event generator based on LEPTO 6.1 [10] and supplemented by generators for quasielastic events and events in the resonance region. The LEPTO

events were generated above a momentum transfer Q^2 of 0.3 GeV^2 and an invariant mass of the hadronic system W^2 of 1.3 GeV^2. They were subsequently passed through a GEANT [11] based full detector simulation. The MC statistics used for the present analysis include samples of 180 000 ν_μ CC and $\bar{\nu}_\mu$ CC events (equivalent to the data statistics), 30 000 ν_e CC and $\bar{\nu}_e$ CC events (about 10 times the data statistics) and 140 000 NC events (more than twice the data statistics). Samples of about 10 000 ν_τ events are used for each of the τ decay channels.

4.1. Event reconstruction

The trajectories of charged particles are reconstructed from the hits in the drift chambers. From these trajectories momenta are estimated using a Kalman filter technique [12] whose transport equations include the magnetic field map and account for the energy loss and multiple scattering in the materiels traversed. Energy losses are initially computed assuming all particles are pions but particles later identified as electrons or positrons by other subdetectors are re-fitted to account for bremsstrahlung (electron fit). Vertices are formed from charged tracks emerging from the same region in space and track parameters are evaluated at the fitted vertex position [12]. For isolated tracks the position of the first hit serves as a vertex. The neutrino interaction point, the primary vertex, is defined as the most upstream vertex with at least one charged track with momentum larger than 500 MeV/c. A typical reconstructed event is shown in Fig. 2.

Charged energy clusters are formed by summing the energy depositions in the calorimeter cells pointed to by charged tracks. Neutral clusters are defined from the remaining contiguous cells. Neutral particles are constructed by connecting them to the primary vertex.

Track segments are reconstructed separately in the two muon stations. Tracks with momentum larger than 2.5 GeV/c, the threshold to reach station 1, are identified as muons if they extrapolate to within 40 cm of at least one of those segments. Electron identification is discussed in Section 6. All tracks not identified as muons or electrons are assumed, at this stage, to be charged pions.

4.2. Kinematic variables

The first step towards the reconstruction of kinematic variables is the definition and reconstruction of the hadronic jet. The difficulty here is to avoid double counting due to secondary interactions within the target volume and due to the energy deposition by charged particles in the calorimeter.

The particles included in the hadronic jet are:
- Charged hadrons associated to the primary vertex. Only the momentum measured in the DC is used, and associated charged clusters are discarded.
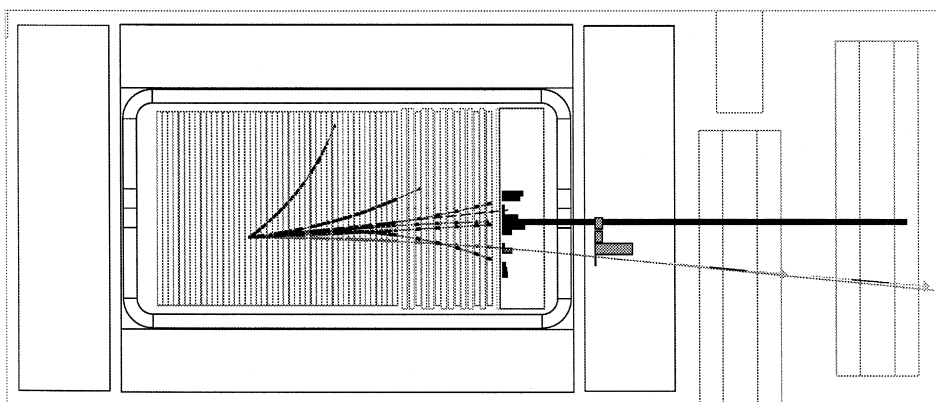

Fig. 2. A fully reconstructed ν_μ-CC candidate. The longest track is a muon matched to the segments in the muon chambers. Energy depositions in the electromagnetic and hadronic calorimeters can also be seen.

- Neutral clusters in the electromagnetic calorimeter.
- V^0's (pairs of oppositely charged tracks making a secondary vertex due to K^0's, Λ's and photon conversions) pointing to the primary vertex.
- Charged hadrons belonging to a secondary vertex with no incoming charged track, i.e. compatible with the interaction of a neutral hadron (n, K_L^0).
- Single charged particles if they extrapolate back linearly to the primary vertex (asymmetric photon conversions).

The hadronic jet formed in this way is measured with an energy resolution of about 25%. It can then be combined with the measured lepton(s), if any, to obtain the kinematic quantities of the event.

The sample of identified ν_μ CC event candidates, where ideally all final state particles can be detected, is used to assess the reconstruction of the kinematic variables in the data sample over the full kinematical range. Satisfactory agreement with Monte Carlo expectations is observed in most variables [13]. These include Q^2, W^2, the Bjorken variables x_B and y_B, and the total visible energy E_{vis} (an approximation to the incident neutrino energy). The transverse variables, measured in a plane perpendicular to the beam, are however the most sensitive to the detailed simulations of the events. In particular, the transverse missing momentum, p_T^m, which results from the difference between the reconstructed hadronic jet and muon transverse momenta, is a direct measure of the resolution of the reconstruction of the hadronic jet. In the data p_T^m has an average value of 820 MeV/c compared to 620 MeV/c in the Monte Carlo simulation. This discrepancy of 200 MeV/c, which is to be compared to an average muon transverse momentum of 1.6 GeV/c, well reproduced by the Monte Carlo, indicates that the hadronic jet reconstruction resolution is underestimated in the simulation. At this stage, the simulation includes a smearing introduced by the initial state nucleon Fermi motion (160 MeV/c on average) and the full detector simulation takes into account the contributions from the detector resolutions (300 MeV/c on average), from reconstruction inefficiencies in the various subdetectors (450 MeV/c on average) and from undetected neutrals escaping the calorimeter (250 MeV/c on average). Additional effects, which can contribute to the hadronic jet resolution, are currently

under study. A more refined nuclear model which includes the simulation of intranuclear cascades and other effects due to the nuclear target is being introduced. A more detailed simulation of the response of the drift chambers is being obtained from a careful study of high statistics data. Preliminary results indicate that these effects, when included, improve the agreement between the data sample and the simulation. However, for the purpose of the analyses presented in this paper, a method has been developed that makes use of the data sample to correct the estimates of the backgrounds and signal efficiencies which are affected by these discrepancies.

4.3. The data simulator

For all the expected τ signals and a large fraction of the expected backgrounds the signal and background efficiencies for cuts involving the hadronic system can be obtained from the *data* themselves. This is achieved by starting from a *measured* ν_μ CC event, removing the identified muon (track and energy deposition), and replacing it by another lepton ℓ.

If ℓ is a neutrino, one obtains fake neutral current events which at these energies, up to charge effects in the hadronic system, simulate actual neutral current events.

If ℓ is an electron, a sample of fake ν_e CC events with about 100 times the statistics of the data is obtained after corrections for the relative ν_e/ν_μ flux and the e/μ efficiency.

Finally, if ℓ is a τ, followed by a simulation of τ decay into the channel being studied, a large sample of fake τ signal events is generated.

All these samples are collectively referred to as the data simulator (DS). The same procedure can also be applied to reconstructed ν_μ CC MC events (Monte Carlo simulator, MCS). A comparison of the result of the MCS to the standard MC yields a powerful cross check of the validity of the muon replacement procedure and the corrections applied, and an estimate of the corresponding systematic uncertainty. On the other hand, a comparison of the DS to the MCS gives a direct measure of the effect of the differences in the hadronic system between the data and the MC, since the leptonic efficiencies are well reproduced.

All signal and background efficiencies, except for ν_μCC events, are obtained through the formula

$$\epsilon = \frac{\epsilon_{MC} \times \epsilon_{DS}}{\epsilon_{MCS}}, \tag{1}$$

which implies that efficiencies for lepton reconstruction and an approximate estimate of hadron reconstruction are obtained from the Monte Carlo (ϵ_{MC}), while the effect of the hadronic jet differences between the data and the MC, which are the main cause of the missing p_T discrepancy, is taken into account through the ratio $\epsilon_{DS}/\epsilon_{MCS}$. This way of calculating efficiencies will be referred to as the data simulator method. It has been checked that efficiencies obtained through this method are indeed stable with respect to variations of the Monte Carlo input (nuclear effects, fragmentation, detector resolution functions) within the quoted uncertainty.

5. τ appearance search

In principle, NOMAD is sensitive to a τ appearance search in all τ decay channels, leptonic and hadronic. The basic concept of the oscillation search in each channel is to use the various MC and data simulator samples to define a set of cuts that reduce the background to an acceptable level and optimize the sensitivity to $\nu_\mu \rightarrow \nu_\tau$ oscillations. All quoted signal and background efficiencies are obtained by the data simulator method, with the exception of the ν_μ CC contribution for which this is not possible. The $\tau \rightarrow \mu\nu\nu$ channel, which could contribute about 10% to the total sensitivity [14], is dominated by the ν_μ CC background. In view of the intrinsic difficulty of the evaluation of the systematic uncertainty on this background, this channel is not included in the results presented in this paper.

5.1. Sources of background

A charged current ν_τ interaction is recognizable due to two effects of the unobserved neutrino(s) from the decay of the τ. The first effect is a missing p_T larger than expected in standard CC events but lower than in NC events and correlated in direction with the charged τ decay products. The second

effect is an underestimate of the leptonic fraction of the final state energy. In addition, the visible decay products of the τ are more isolated from the recoil jet than fragments of the hadron jet being mistakenly identified as τ decay products.

In the hadronic decay channels the NC and CC backgrounds must be suppressed kinematically. In addition, the CC background must be reduced through an efficient lepton veto. In the electron channel the dominant background arises from mismeasured ν_e CC events, which must again be reduced by kinematical cuts, while most of the NC background is removed by tight lepton quality and moderate isolation cuts.

Backgrounds from NC and ν_e CC events and all signal efficiencies can be controlled by comparing the MC, MCS, and DS samples. For all channels the simulation of the processes yielding background to the τ search is checked by comparing the estimates of these processes in kinematic regions where no signal is expected. Moreover, because of the small $\bar{\nu}_\mu$ component of the beam, essentially no $\bar{\nu}_\tau$ and hence no τ^+ are expected in the data. The estimates for some backgrounds (e.g. NC) can therefore be checked further by performing an analysis in the τ^+ channel. Note that more positive than negative background is expected from these sources because of the more favourable charge configuration.

5.2. General analysis strategy

The general analysis procedure followed for all τ decay channels can be summarized as follows.

A set of event quality cuts is applied based on the charge balance at the primary vertex and the momentum errors. This removes at most 15% of the events.

For each channel, two separate analyses are carried out: one using events with ≥ 1 tracks at the primary vertex in addition to the τ decay products (the DIS analysis) and the other using events with 0 or 1 or 2 additional tracks (the low multiplicity analysis). Since events with 1 or 2 additional tracks can enter both analyses a cut on the hadronic momentum, p^h, is applied to make the two studies complementary. The choice of the cut ($p^h > 1.5$ GeV$/c$ for the DIS analysis and $p^h < 1.5$ GeV$/c$ for the low multiplicity analysis) is intended to en-

rich the low multiplicity sample in quasi-elastic and resonance events.

The visible decay products (X_v) of potential τ candidates are identified. If a primary lepton (muon or electron) is reconstructed, X_v is taken to be that lepton and the event is used for the $\tau \to \mu$ or $\tau \to e$ analysis ($X_v = \mu$ or e). If no lepton candidates are found, the event is considered for the $\tau \to$ hadron channels. X_v is then taken to be a charged hadron for the one prong analysis ($X_v = \pi$), a $\pi^- \pi^0$ combination for the ρ analysis ($X_v = \pi^- \pi^0$) or a suitable 3-hadron combination for the 3-prong analysis ($X_v = 3\pi$).

5.3. Definition of variables

The following kinematic variables are defined and used to separate the signal from the background:

· p_T^m, defined as $|\boldsymbol{p}_T^{X_v} + \boldsymbol{p}_T^h|$ and interpreted as a measurement of the transverse momentum of the neutrino(s) from τ decay.

· $p_T^{X_v}$ and θ^{X_v}, the transverse component of $\boldsymbol{p}^{X_v}$ and angle in the laboratory of the decay product with respect to the beam direction.

· the transverse mass, M_T, given by $M_T^2 = 4 p_T^{X_v} p_T^m \sin^2(\phi_{X_v m}/2)$, where $\phi_{X_v m}$ is the angle in the transverse plane between the visible and invisible τ decay products. For true τ events, $M_T \leq m_\tau$, up to detector resolution effects.

· Q_T, the component of $\boldsymbol{p}^{X_v}$ perpendicular to the total visible momentum vector (including X_v). Large Q_T implies that X_v is well isolated from the remaining hadronic jet.

· Q_{Lep}, the component of $\boldsymbol{p}^{X_v}$ perpendicular to the hadronic jet direction (excluding X_v). Its function is very similar to Q_T, but it is more useful when the momentum of the recoil jet, p^h, is small.

· $\theta_{X_v h}$, the angle between the hadronic jet and X_v.

· $\phi_{X_v h}$, ϕ_{mh}, the angles in the transverse plane between the hadronic recoil vector and the visible and invisible decay product, respectively [15].

· Ratios of linear combinations of p_T^m, $p_T^{X_v}$, and p_T^h, equivalent to functions of the previous two angles described.

For some channels, combinations of these and other variables are used to build a likelihood ratio. The likelihood functions entering this ratio are approximated by the product of one or two dimensional probability density functions of these variables. As is common practice, the logarithm of this ratio has been used. The actual set of variables used for each decay channel will be described where appropriate.

5.4. τ efficiency

For each channel the τ efficiency is obtained using the data simulator method outlined above. The values quoted are calculated relative to the number of events with ≥ 1 additional tracks for the DIS analysis and ≤ 2 additional tracks for the low multiplicity analysis. The quoted uncertainties include uncertainties in the simulation of the hadronic system and the statistical uncertainty of the Monte Carlo and data simulator samples used. The cuts and procedures specific to the analysis of each channel are presented in the following sections.

6. $\tau^- \to e^- \bar{\nu}_e \nu_\tau$ decays

Topologically, an electron candidate is defined as a drift chamber track traversing the transition radiation detector and pointing to an energy deposition in the lead glass. At first, the momentum of the candidate, p, is taken to be that computed at the origin of the track using the electron fit. The energy of the electron, E, is taken to be the energy of the calorimeter cluster it points to, augmented by the energy of all the photons that could have come from bremsstrahlung emission. Only candidates associated to the primary vertex and with $p > 1.5$ GeV/c are considered. To reject charged hadrons the following requirements are imposed on a candidate:

· An energy deposition in the TRD [7] such that the probability for a pion to have deposited that much energy is $< 10^{-3}$. No other primary track is allowed to hit the same TRD tubes.

· A preshower pulse height well above that of a minimum ionizing particle [8].

· A calorimeter cluster shape consistent with that of an electromagnetic shower as measured in an electron test beam [8].

· The energy and the momentum of the candidate to agree within
$-0.2 < (E - p)/(E + p) < 0.2$.

Overall, a charged pion rejection factor of the order of 10^4 is achieved. Another source of background to

primary electrons arises from photon conversions. Most of these are rejected by the primary vertex association requirement. In order to reduce this background further, the invariant mass formed between the electron candidate and any other close track of opposite charge must be > 120 MeV/c^2. After these cuts, only one out of 3000 π^0's yields photon conversions or Dalitz decays where one of the secondaries is mistaken for a primary electron.

This yields a rejection factor against neutral currents of 500 and an efficiency of 37% for prompt electrons from ν_e CC. The effect of the primary electron identification cuts is demonstrated in Table 1. For the final electron candidates, the momentum vector is formed using the initial direction of the electron momentum and assigning the energy as defined earlier as its magnitude.

6.1. DIS search

The search for $\tau^- \to e^- \bar{\nu}_e \nu_\tau$ decays initiates by looking for a prompt electron and requiring no other lepton candidate in the event. The effect of the cuts described below are also shown in Table 1. Most surviving electrons from NC events (e.g. Dalitz decays or photon conversions) are rejected by selecting events in the region of the $\theta_{eh} - Q_{Lep}$ plane, shown in Fig. 3, characteristic of isolated electrons. The remaining event sample is then entirely dominated by primary electrons from ν_e CC interactions. These are reduced by requiring consistency with the τ mass ($0.2 < M_T < 1.8$ GeV/c^2) and by rejecting electrons

with $Q_{Lep} > 5$ GeV/c. The effectiveness of this last cut, demonstrated in Fig. 3, can be attributed to the reduction of the electron momentum due to the τ 3-body decay.

For the remaining events, an approximate likelihood function is built multiplying two one-dimensional distributions, p^e and p_T^e/p_T^h, and two two-dimensional distributions, ϕ_{eh} vs ϕ_{mh} and p_T^m vs E_{vis} (Fig. 4). The resulting likelihood ratio L_{τ/ν_e} estimates the relative probability of an event to be of $\tau \to e$ or of ν_e CC origin and is shown in Fig. 5. A cut at $\log(L_{\tau/\nu_e}) > 6.5$ is seen to reject the ν_e CC background by two orders of magnitude while keeping 46% of the signal. One event remains in the ν_e CC Monte Carlo sample, corresponding to a total background estimate of $0.6^{+0.7}_{-0.6}$ events. The resulting τ efficiency is $(4.6 \pm 0.9)\%$. In order to avoid biases, the Monte Carlo sample used to calculate this efficiency was different from the one used to generate the reference distributions needed in the likelihood calculation. No τ^- candidate is observed in the data. A single positive event is observed, consistent with an expectation of $0.4^{+1.1}_{-0.4}$, which includes events from charm $\to e^+$ decays with an undetected muon.

6.2. Low multiplicity search

The low multiplicity analysis is divided into 1-track events and 2 or 3-track events. The cuts used in the analysis are listed below. Some of them are tighter for the 1-track sample and this tighter value is shown in parentheses. Clearly for the 1-track events

Table 1
The effect of the cuts (described in the text) used in the $\tau \to e\nu\nu$ DIS analysis on simulated τ signal events, and background ν_e CC, ν_μ CC and NC events, as well as the data. In the ν_μ CC and NC columns, small contributions from $\bar{\nu}$ are included. The ν_τ column shows the τ efficiency. The background samples have been suitably normalized to the data. The sum of all 3 backgrounds is also shown, as is the effect of the cuts on the positive control sample

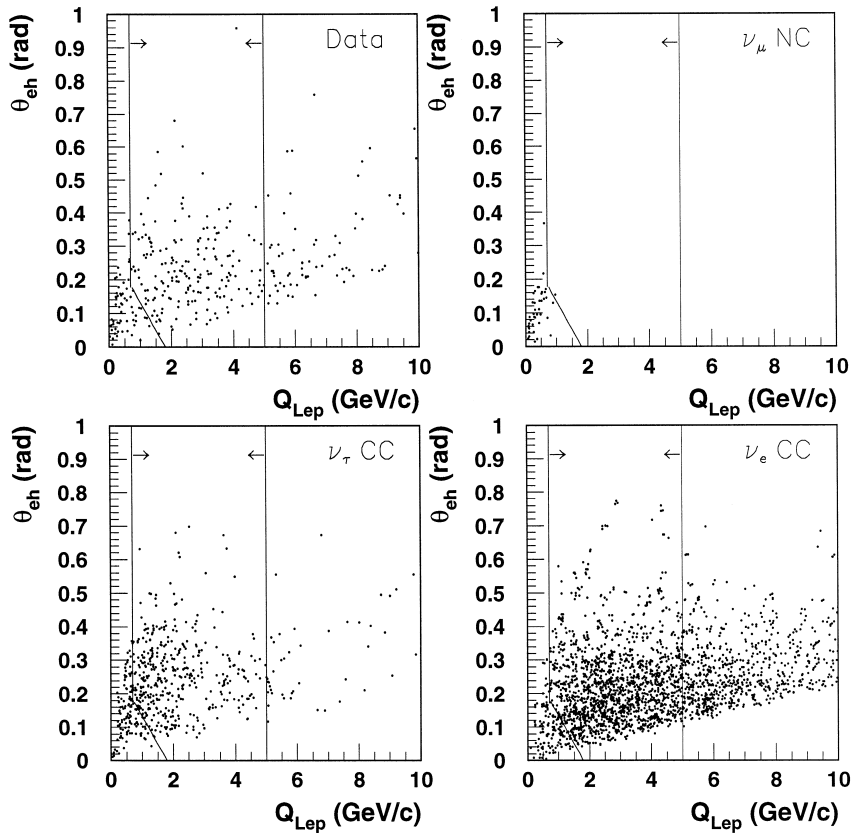| Sample	ν_τ MC	ν_e CC	$\bar{\nu}_e$ CC	ν_μ CC		NC		Sum		Data	
Charge	$-$	$-$	$+$	$-$	$+$	$-$	$+$	$-$	$+$	$-$	$+$
$N_{\text{track}} \geq 2$	0.950	1836	212	162000		47804		211852		208776	
Electron ID	0.289	684	46	57	87	103	77	844	210	897	251
$\theta_{eh} - Q_{Lep}$	0.123	152	11	0.0	6.3	1.6	2.8	154	20	198	18
M_T	0.100	57	2.2	0.0	5.9	0.0	0.0	57	8.1	65	8
Likelihood	0.046	0.6 ± 0.6	0.4 ± 0.4	0.0	0^{+1}_{-0}	$0^{+0.4}_{-0}$	$0^{+0.4}_{-0}$	$0.6^{+0.7}_{-0.6}$	$0.4^{+1.1}_{-0.4}$	0	1

Fig. 3. The $\theta_{eh} - Q_{Lep}$ distributions for data and for Monte Carlo NC, ν_τ CC, and ν_e CC events. The region used in the $\tau^- \to e^- \bar{\nu}_e \nu_\tau$ DIS search is the one bounded by the two lines.

with no neutral energy and no secondary tracks, no hadronic vector could be built and only cuts involving the kinematic properties of the electron could be applied. To reject ν_eCC background the following cuts are used: $\theta^e < 200(150)$ mrad, $p^e < 15(10)$ GeV/c, $p_T^m > 0.5$ GeV/c, $y_B(= 1 - p_e/E_{vis}) > 0.10$ and a cut in the $\phi_{eh} - \phi_{mh}$ plane. The $\phi_{eh} - \phi_{mh}$ distributions for the signal and ν_e CC background are similar to the ones drawn in Fig. 4 for the DIS analysis. Electrons from $\nu_\mu e$ interactions are eliminated with a cut of $\theta^e > 35$ mrad for single track topologies. The rejection of ν_μNC background is achieved by requiring: $p_T^m < 3.0$ GeV/c, $M_T < 1.9$ GeV/c^2, $y_B < 0.75$, and isolation cuts: $0.5 < Q_{Lep} < 11.5$ GeV/c and $\theta_{eh} > 0.25$ rad. No τ^- candidate survives in the data for a τ efficiency of $(3.4 \pm 0.6)\%$ in the low multiplicity events. The expected background is $0.5^{+0.6}_{-0.2}$ events coming mostly from events

in the one-track sample. One τ^+ candidate is observed with an expected background of 1.1 ± 0.7.

7. $\tau^- \to h^-(n\pi^0)\nu_\tau$ decays

In the search for oscillations in the $\tau^- \to h^-\nu_\tau(+n\pi^0)$ decay channel, the following requirements are applied to hadrons in order to ensure that they are not mismeasured muons or electrons:

· No associated raw muon chamber hits in at least one projection.
· Energy deposition in the ECAL and HCAL inconsistent with a minimum ionizing particle.
· Energy deposition in the TRD, the PS and/or the ECAL inconsistent with an electron.

Throughout the rest of this paper the $h^\pm$ ($\pi^\pm, K^\pm$) are referred to as $\pi^\pm$ for simplicity.
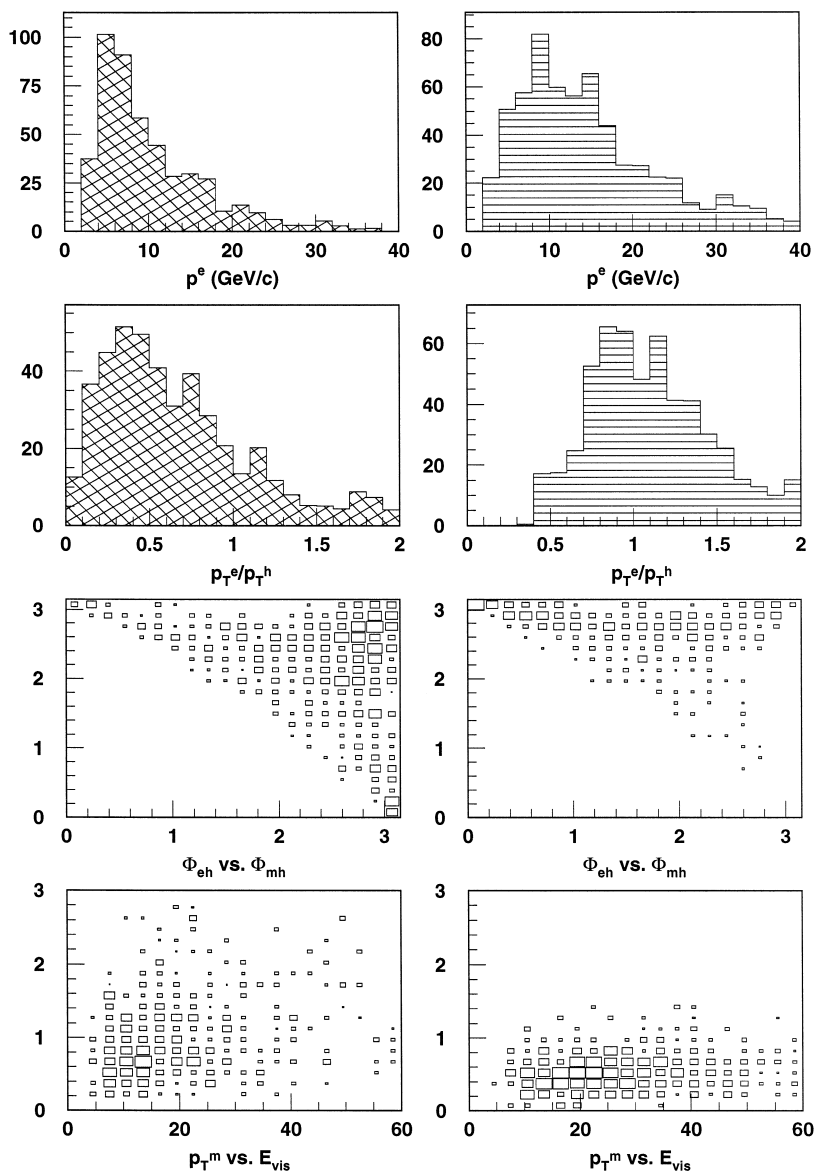
Fig. 4. The distributions in p^e, p_T^e/p_T^h, ϕ_{eh} vs ϕ_{mh} and p_T^m vs E_{vis} used to build the likelihood ratio for Monte Carlo τ events (left column) and Monte Carlo ν_e CC events (right column) in the $\tau^- \to e^- \bar{\nu}_e \nu_\tau$ DIS search.

7.1. DIS search

For the DIS analysis the event selection requirements imposed are:

· a leading primary track with negative charge (π^- candidate) capable of reaching the muon detector with momentum $p^\pi > 3$ GeV/c.

· no track with $p_T > 0.8$ GeV/c, well isolated from the hadronic jet, that could have escaped muon or electron detection.

These cuts eliminate most of the background from ν_μ, $\bar{\nu}_\mu$ and ν_e CC events. Their effect and that of subsequent cuts on the data and on all the simulated event samples is shown in Table 2. A cut of $p_T^m <$
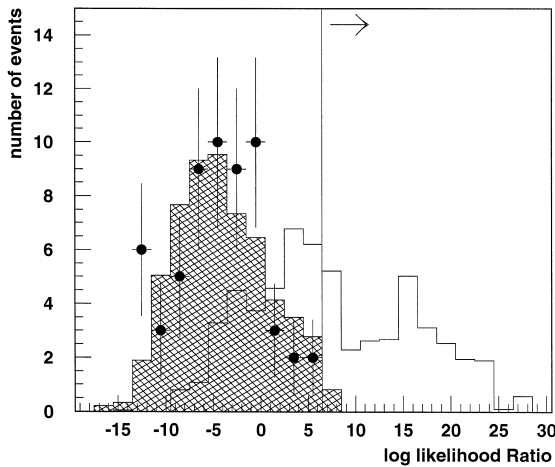
Fig. 5. The likelihood ratio L_{τ/ν_e} defined in the text, for the data (solid points), the background obtained using the data simulator method (hatched area) and the simulated τ signal (histogram). The region used in the $\tau^- \to e^- \bar{\nu}_e \nu_\tau$ DIS search is also shown.

2.0 GeV/c reduces the NC background and a cut on the transverse mass of $M_T < 2.5$ GeV/c^2 retains only events that are kinematically consistent with τ decay.

The remaining candidates are mostly NC events where one of the tracks in the hadronic jet is mistaken for the hadron from τ decay. As shown in Fig. 6 and Table 2, imposing a cut of $Q_T > 1.7$ GeV/c removes the remaining background, while retaining a τ efficiency of $(1.20 \pm 0.25)\%$ for $\tau \to \pi\nu$ decays, $(0.30 \pm 0.09)\%$ for $\tau \to \rho\nu$ decays and negligible efficiency for the remaining hadronic $\tau \to$ 1 prong decay channels. Applying these cuts to the data, no candidates are observed.

The muon veto inefficiency is measured to be $(0.6 \pm 0.1) \times 10^{-4}$ using a large sample of muons originating from neighbouring test beams and traversing the NOMAD detector outside the neutrino spills. The background from unidentified high momentum muons originating in ν_μCC events is then obtained from the data, by removing the muon veto cuts, and applying the measured muon veto efficiency to the surviving number of events. Combining this with the contribution of muons below detection threshold from the MC, a background estimate of $0.2^{+1.2}_{-0.1}$ events is obtained. No event survives in the simulated neutral current and ν_eCC samples, leading

to background estimates from these sources of $0.0^{+1.4}_{-0.0}$ and $0.0^{+0.1}_{-0.0}$, respectively. The total expected background is then $0.2^{+1.8}_{-0.1}$ events. Application of the same procedure to τ^+ candidates yields 1 event for $1.7^{+1.9}_{-1.2}$ expected.

Because of the hard Q_T cut applied to the single π^- candidate in this analysis the $\tau \to \rho\nu$ events selected here are different from those selected by the dedicated $\rho^- \to \pi^- \pi^0$ analysis described in Section 8. The sensitivities to the $\tau \to \rho\nu$ channel of the two analyses are therefore additive.

7.2. Low multiplicity search

In the low multiplicity analysis the candidate pion is taken to be the track satisfying the largest number of the following criteria: highest momentum, largest $\phi_{\pi h}$ and largest Q_{Lep}. In order to select events with the topology characteristic of quasielastic and resonance events, a cut on $W^2 - m_p^2 \le 1.5$ GeV^2/c^4, where m_p is the proton mass, is applied. A cut $0.5 \le p_T^\pi \le 1.2$ GeV/c preferentially selects pions from τ decays, where the p_T arises from the τ mass (Fig. 7). For the one track sample, a cut on the pion direction ($\theta^\pi < 100$ mrad) is applied. For the 2 or 3 track sample, the recoiling hadronic jet direction is
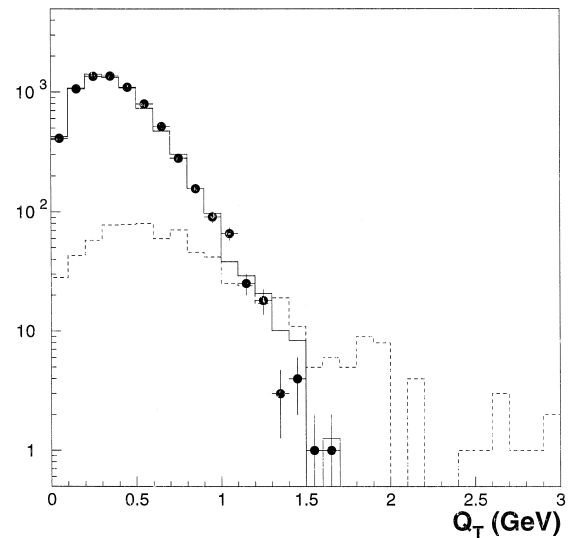

Fig. 6. The Q_T distribution in the DIS analysis for the data (solid points), the background (solid line) and the simulated $\tau^- \to \pi^- \nu_\tau$ signal (dashed line)

Table 2
The effect of the cuts (described in the text) used in the $\tau \to \pi\nu$ DIS analysis. The organization is the same as in Table 1

Sample	ν_τ MC	ν_e CC		ν_μ CC		ν_μ NC		Sum		Data	
Charge	−	−	+	−	+	−	+	−	+	−	+
≥ 1 cand.	0.467	453	159	116040	40702	11106	10178	127599	51039	140794	47964
Quality	0.436	418	149	110832	39400	10228	9460	121478	49009	130591	45127
Veto CC	0.264	41	64	1266	1988	7555	6984	8862	9436	9469	10139
p_T^m, M_T	0.222	35	55	1137	1795	4820	4284	5992	6134	6725	7312
Q_T	0.012	$0.0^{+0.1}_{-0.0}$	0.5 ± 0.2	$0.2^{+1.2}_{-0.1}$	1.2 ± 1.2	$0.0^{+1.4}_{-0.0}$	$0.0^{+1.4}_{-0.0}$	$0.2^{+1.8}_{-0.1}$	$1.7^{+1.9}_{-1.2}$	0	1

measured and cuts on the transverse mass and on the separation between the pion candidate and the recoil hadron jet are used. The low multiplicity analysis yields one τ^- candidate. The efficiency is $(3.5 \pm 0.7)\%$ for the $\tau \to \pi\nu$ decays and $(0.5 \pm 0.1)\%$ for $\tau \to \rho\nu$ decays. The background estimated from the data simulator method is $0.1^{+0.3}_{-0.1}$ events. The τ^+

control sample yields 6 candidates in the data for an expectation of 8.8 ± 3.5 from the simulation. The background is much smaller in the negative than in the positive channel because the background is dominated by single track events and charge conservation prohibits hadronic systems consisting of a single negative track.
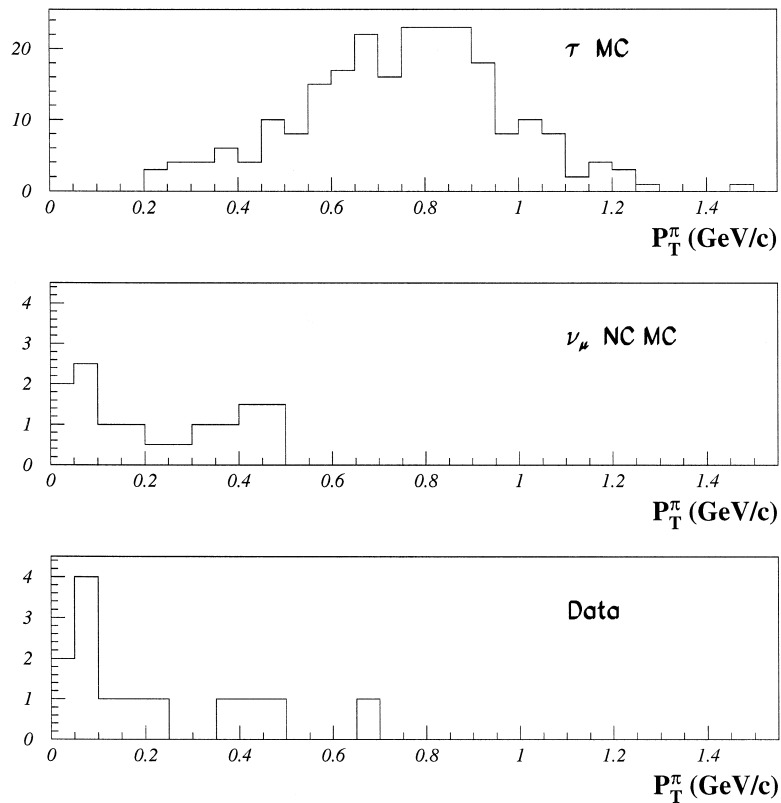

Fig. 7. The p_T^π distribution in the low multiplicity analysis for the $\tau^- \to \pi^- \nu_\tau$ and NC Monte Carlo samples and for the data, after application of all other cuts.

8. $\tau^- \to \rho^- \nu_\tau$ decays

Only a DIS analysis was performed in this channel. It is based on the reconstruction of the $\rho^- \to \pi^- \pi^0$. Events in which both photons from the π^0 decay reach the calorimeter without converting in the drift chambers (37%) are considered. They can be detected either as two distinct clusters (2NCL) in which case the π^0 can be reconstructed or, when they coalesce, as a single cluster (1NCL). In order to select a sample of events with a better reconstruction, a tighter fiducial cut ($z < 310$ cm) is used in this analysis. An approximate likelihood ratio, L_ρ, is used to select, in each event, the most likely $\pi^- \pi^0$ combination to originate from a ρ from τ decay. It is based on the $\pi^- \pi^0$ opening angle and invariant mass, on the ratio of the ρ candidate energy to the total visible energy and on the angle between the ρ and the hadronic jet direction. For the 2NCL analysis the invariant mass and the opening angle of the two photons are also included. Selecting the highest likelihood combination correctly identifies the ρ in 80% of the events. The same combination of variables is used to build a second approximate likelihood ratio, $L_{\tau/NC}$, to discriminate between neutral currents and τ decays. Cuts on the transverse plane variables, on $Q_T^\rho > 1.5$ GeV/c and on $\log(L_{\tau/NC}) > 2.2$ achieve this result.

Unidentified leptons in charged current events can result in a background as they can combine with a π^0 to simulate a ρ from a τ decay. The ν_μCC background is reduced by requiring that the two highest p_T tracks in the event as well as the π^- candidate do not miss the muon chambers and are inconsistent with being a muon both in the muon chambers and in the calorimeters. Background from ν_eCC events is reduced by requiring that the π^- candidate deposit less than 15 GeV in the lead glass and that the two highest p_T tracks are not identified as electrons in the TRD.

The efficiency is calculated to be $(0.8 \pm 0.2)\%$. No candidate event is observed in the data for an estimated background of $0.5^{+2.1}_{-0.3}$. Applying the same analysis to τ^+ candidates yields 2 events with an expectation of $3.7^{+1.6}_{-1.5}$.

9. $\tau^- \to \pi^- \pi^+ \pi^- \nu_\tau$ decays

The search for $\nu_\mu \to \nu_\tau$ oscillations using the $\tau^- \to \pi^- \pi^+ \pi^- \nu_\tau$ decay channel [16] has the feature of providing additional kinematical constraints compared to the one-prong channels, since most of these decays occur via the a_1 resonance and leave little energy for the associated neutrino.

9.1. DIS search

Two approximate likelihood ratios are formed, both built from the mass of the 3π system ("a_1" mass), the masses of the $\pi^+ \pi^-$ subsystems ("ρ" mass), the ratio of the energy of the 3π system to the total visible energy (y_B), the maximum (lab) opening angle among the three pions (θ_{max}), and an isolation variable (θ_{isol}) equal to the smallest angle between any of the three candidate decay products and any of the remaining hadrons. The first likelihood ratio, $L_{3\pi}$, is used to select the most likely 3π combination to be the τ decay in a given event, and picks the right combination in 73% of all simulated

Table 3
The effect of the cuts (described in the text) used in the $\tau \to 3\pi\nu$ DIS analysis. The organization is the same as in Table 1

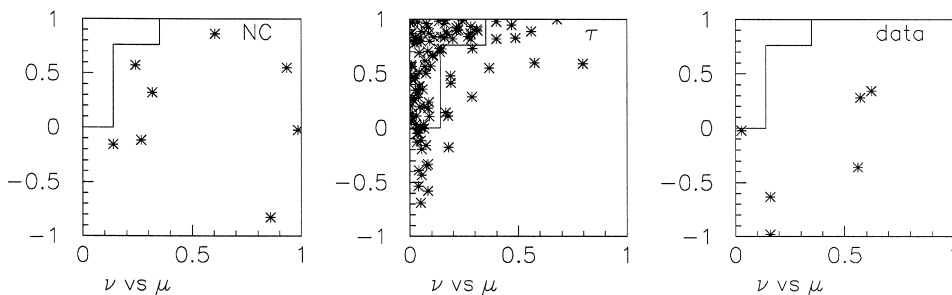| Sample	ν_τ MC	ν_eCC	ν_μ CC		ν_μ NC		Sum		Data	
Charge	−	−	−	+	−	+	−	+	−	+
3π combination										
with Q = $\mp$1	0.590	907	19260	19917	20595	20980	40762	40987	37408	40590
ν_τ NC	0.091	6	144	397	288	459	438	856	395	677
Q_T	0.044	3	40	145	16	17	59	162	51	127
$\hat{\nu} - \hat{\mu}$	0.031	2	34	119	$0.0^{+0.8}_{-0.0}$	0.8	36	119	25	83
μ veto	0.017	1.0	0.2	0.8	$0.0^{+0.4}_{-0.0}$	0.4	1.0	1.2	3	4
e veto	0.016	0.2 ± 0.1	0.2 ± 0.1	0.8 ± 0.4	$0.0^{+0.4}_{-0.0}$	0.4 ± 0.4	$0.4^{+0.4}_{-0.1}$	1.2 ± 0.6	0	2

Fig. 8. The distribution in $\hat{\nu} - \hat{\mu}$ (defined in the text) for the Monte Carlo ν_μ NC and $\tau \to 3\pi\nu$ events and for the data, after application of all other cuts. The region used in the τ search is the one shown in the top left hand corner of the three plots.

$\tau \to 3\pi$ events, and in 100% of the events surviving all other cuts. The second variable $L_{\tau/NC}$ estimates the relative probability for the selected combination to come from a τ as opposed to a random combination from a neutral current event. Only events with $\log(L_{\tau/NC}) > 2$ are retained. The effect of this cut and of the other cuts used in this analysis is shown in Table 3. The number of neutral current events is reduced by an isolation cut, $Q_T^{3\pi} > 1.2$ GeV/c. The remaining events in the simulated neutral current samples are rejected by a cut on the $\hat{\nu} - \hat{\mu}$ plane, where $\hat{\nu} = (p_T^{3\pi} - p_T^m)/(p_T^h)$ and $\hat{\mu} = (p_T^{3\pi} + p_T^m - p_T^h)/(p_T^{3\pi} + p_T^m + p_T^h)$. τ events will tend to have $\hat{\nu} \sim 1$ and $\hat{\mu} \sim 0$ since for them $(p_T^{3\pi} + p_T^m) \sim p_T^h$, whereas neutral current events are much more uniformly distributed (Fig. 8).

The remaining background is caused by CC events in which the charged lepton is not identified. To reduce this background the two highest p_T tracks are required to be inconsistent with being a muon in both the muon chambers and the calorimeter, and to be inconsistent with an electron. If this information is not available because the relevant tracks miss the lepton detectors, the event is rejected.

By releasing the cut on $L_{\tau/NC}$ to increase the statistics, it is found that 0.7% of the ν_μCC events survive the muon veto. The number of background ν_μCC events in the data is then estimated to be 0.2 ± 0.1. Note that the muon veto described here is less effective than the one used in the single pion analysis described earlier because the lower pion momenta in the $\tau \to 3\pi$ decay imply that the muons that would simulate a pion from τ decay are those of low momentum, for which the muon spectrometer has a lower acceptance. The contributions to the

background from ν_eCC and ν_μNC are calculated to be 0.2 ± 0.1 and $0.0^{+0.4}_{-0.0}$ events, respectively. The overall background is then $0.4^{+0.4}_{-0.1}$ events while no τ^- candidate is found in the data. The efficiency for $\tau^- \to \pi^- \pi^+ \pi^- \nu_\tau$ is (1.6 ± 0.3)%. Three-prong decays with additional neutrals have not yet been included in this analysis. The background prediction is confirmed by a study of τ^+ candidates: 2 events are observed for 1.2 ± 0.6 expected.

9.2. Low multiplicity search

In this analysis, in which three prong decays with additional neutrals are included, criteria similar to the ones described above and based on the invariant mass and topology of the 3π system and on the transverse mass are used to select the most likely 3π combination and to reject the NC and CC background. No candidate is observed in the data for an efficiency of (2.0 ± 0.3)% and an expected background of $0.4^{+0.6}_{-0.4}$. The same analysis applied to τ^+ candidates yields 14 events for an expectation of 11 ± 4.

10. The limit for $\nu_\mu \to \nu_\tau$ oscillations

We express the result of the measurements described above as a frequentist confidence interval [17] by optimally combining the measurements for each channel, taking into account the number of observed signal events, the expected background and its uncertainty, and the number of expected signal

Table 4

Summary of backgrounds and efficiencies for all analyses described. DIS and LM refers to the DIS and low multiplicity analyses for each decay channel. The column τ^- summarizes the observed number of τ^- candidate events (obs.) and the corresponding predicted background (est. backgr.) for each channel. The column τ^+ contains the equivalent numbers for "wrong sign" candidates. The corresponding τ^- selection efficiencies (ϵ) and τ branching ratios (Br) are also listed. Finally, the maximal number of expected signal events (N_{max}), as computed from Eq. (2), is indicated for each channel

analysis	τ^-		τ^+		$\epsilon(\%)$	$Br(\%)$	N_{max}
	obs.	est. backgr.	obs.	est. backgr.			
$\tau \to e$ DIS	0	$0.6^{+0.7}_{-0.6}$	1	$0.4^{+1.1}_{-0.4}$	4.6 ± 0.9	17.8	635
$\tau \to e$ LM	0	$0.5^{+0.6}_{-0.2}$	1	1.1 ± 0.7	3.4 ± 0.6	17.8	218
$\tau \to \pi(\pi^0)$ DIS	0	$0.2^{+1.8}_{-0.1}$	1	$1.7^{+1.9}_{-1.2}$	1.2 (0.3)	12.0(25.8)	173
$\tau \to \pi(\pi^0)$ LM	1	$0.1^{+0.3}_{-0.1}$	6	8.8 ± 3.5	3.5 (0.5)	12.0(25.8)	198
$\tau \to \rho$ DIS	0	$0.5^{+2.1}_{-0.3}$	2	$3.7^{+1.6}_{-1.5}$	0.8 ± 0.2	25.2	128
$\tau \to 3\pi$ DIS	0	$0.4^{+0.4}_{-0.1}$	2	1.2 ± 0.6	1.6 ± 0.3	9.8	122
$\tau \to 3\pi(n\pi^0)$ LM	0	$0.4^{+0.6}_{-0.4}$	14	11 ± 4	2.0 ± 0.3	14.9	108
all τ	1	$2.7^{+3.0}_{-0.8}$	27	28 ± 6		70.5	1582

events if the oscillation probability were unity. This last quantity is given by

$$N_{max} = N_\mu \times (\sigma_\tau/\sigma_\mu) \times Br \times \epsilon, \qquad (2)$$

where:

· N_μ is the number of ν_μ CC interactions, after correction for muon identification efficiency, in the subsample of ν_μ CC events corresponding to the conditions of the analysis in question. The DIS and low multiplicity analysis subsamples, which overlap partially, consist of 162 000 and 68 000 events, respectively.

· (σ_τ/σ_μ) is the suppression factor of the ν_τ cross section due to the difference between the τ and μ masses. It is calculated to be 0.48 for scaling and 0.73 for non-scaling processes, resulting in 0.48 for the DIS analysis and 0.53 for the low multiplicity analysis.

· Br is the branching ratio and ϵ is the selection efficiency for the τ decay channel in question.

These quantities are summarized in Table 4. The systematic uncertainty on N_{max} is about 15%, resulting mostly from the uncertainty on the efficiency calculations. The effect of this systematic uncertainty on the limit calculation is negligible in the frequentist approach [18].

To construct the confidence interval, we follow the procedures of Ref. [17], replacing the likelihood ratio with a generalized form [19] to account for the

uncertainties in the background estimation. The resulting 90% confidence level upper limit corresponds to 3.3 events and thus leads to an upper limit on the oscillation probability of

$$P_{osc}(\nu_\mu \to \nu_\tau) < 3.3/1582 = 2.1 \times 10^{-3}, \qquad (3)$$

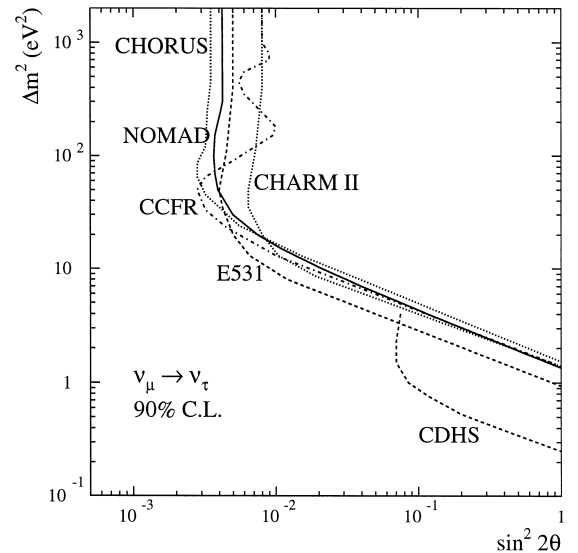which corresponds to $\sin^2 2\theta_{\mu\tau} < 4.2 \times 10^{-3}$ for large

Fig. 9. The $\Delta m^2 - \sin^2 2\theta$ plane. The region excluded by NOMAD at 90% c.l. (solid line) is shown together with limits set by other experiments [5,20,21].

Δm^2 and to the exclusion region in the $\Delta m^2 - \sin^2 2\theta$ plane shown in Fig. 9. A similar result [5] has also been presented by the CHORUS collaboration [20].

Since the number of observed events is fewer than the estimated background, the sensitivity of the experiment, defined as the average upper limit that would be set by an ensemble of experiments with the same expected background in the absence of signal [17], is higher than the quoted result. A Monte Carlo simulation of 1000 such experiments yields an oscillation probability sensitivity of 3.0×10^{-3}. The likelihood to obtain a probability of 2.1×10^{-3} or lower is 35%.

11. Conclusion

Based on an analysis of 17% of the data already collected, NOMAD has now set an upper limit on $\sin^2 2\theta_{\mu\tau}$ at high Δm^2 of 4.2×10^{-3} at 90% c.l.. It is expected that by using the remainder of the data, by adding the data to be collected during the approved 1998 run and by improving the efficiency for the signal the sensitivity of the experiment will be improved substantially.

References

[1] See, for instance, M. Nakahata, Neutrino Masses and Oscillations, Plenary talk at the International Europhysics Conference on High Energy Physics, Jerusalem, Israel, 19–26 August 1997.

[2] LSND Collaboration, C. Athanassopoulos et al., Phys. Rev. C 54 (1996) 2685; Phys. Rev. Lett. 77 (1996) 3082; LA-UR-97-1998, UCRHEP-E191, submitted to Phys. Rev. C.

[3] H. Harari, Phys. Lett. B 216 (1989) 413; J. Ellis, J.L. Lopez, D.V. Nanopoulos, Phys. Lett. B 292 (1992) 189.

[4] NOMAD Collaboration, P. Astier et al., CERN-SPSLC/91-21 (1991); Addendum 1, CERN-SPSLC/91-48 (1991); Addendum 2, CERN-SPSLC/91-53 (1991).

[5] E531 Collaboration, N. Ushida et al., Phys. Rev. Lett. 57 (1986) 2897.

[6] NOMAD Collaboration, J. Altegoer et al., Nucl. Instr. and Meth. A 404 (1998) 96.

[7] G. Bassompierre et al., Nucl. Instr. and Meth. A 403 (1998) 363; G. Bassompierre et al., LAPP-EXP-97-06, 1997, submitted to Nucl. Instr. and Meth.

[8] D. Autiero et al., Nucl. Instr. and Meth. A 372 (1996) 556; A 373 (1996) 358; A 387 (1997) 352.

[9] M.C. Gonzales-Garcia, J.J. Gomez-Cadenas, Phys. Rev. D 55 (1997) 1297; B. Van de Vijver, P. Zucchelli, Nucl. Instr. and Meth. A 385 (1997) 91.

[10] G. Ingelman, The LUND MC for Deep Inelastic Lepton-Nucleon Scattering, LEPTO 6.1 Physics at HERA, October 1991; T. Sjöstrand, Computer Physics Commun. 39 (1986)

---

[5] Statistical methods used by other experiments [5,20,21] would yield more stringent limits for our experiment. For example, summing up all τ decay channels and assuming a precisely known total background of 2.7 events the method described in Ref. [22] would give an upper limit on $\sin^2 2\theta_{\mu\tau}$ of 3.7×10^{-3} @90% c.l..

347; H.U. Bengtsson, T. Sjöstrand, JETSET, Computer Physics Commun. 43 (1987) 367.

[11] The NOMAD simulation program is based on GEANT 3.21, CERN Program Library Long Writeup W5013.

[12] R. Frühwirth, Nucl. Instr. and Meth. A 262 (1987) 444, and references therein.

[13] B. Schmidt, Ph.D. thesis, University of Dortmund, 1997.

[14] V. Valuev, NOMAD Collaboration, proceedings of the International Europhysics Conference on High Energy Physics, Jerusalem, Israel, 19–26 August 1997, to be published; J. Long, Ph.D. thesis, Johns Hopkins University, Baltimore, Maryland, USA, 1997.

[15] C. Albright et al., Phys. Lett. B 84 (1979) 123.

[16] J.A. Hernando-Morata, Ph.D. thesis, University of Valencia, 1997.

[17] G.J. Feldman, R.D. Cousins, Phys. Rev. D 57 (1998) 3873.

[18] R.D. Cousins, V.L. Highland, Nucl. Instr. and Meth. A 320 (1992) 331.

[19] M.G. Kendall, A. Stuart, The Advanced Theory of Statistics, vol. 2, Inference and Relationship 3rd ed., Hafner Publishing, New York, 1973, p. 234, Eq. 24.4.

[20] CHORUS Collaboration, E. Eskut et al., Phys. Lett. B 424 (1998) 202.

[21] CHARM-II Collaboration, M. Gruwe et al., Phys. Lett. B 309 (1993) 463; CCFR Collaboration, K.S. McFarland et al., Phys. Rev. Lett. 75 (1995) 3993; CDHS Collaboration, F. Dydak et al., Phys. Lett. B 134 (1984) 281.

[22] O. Helene, Nucl. Instr. and Meth. 212 (1983) 319.